Catal Lett (2014) 144:723–735
DOI 10.1007/s10562-014-1201-0

Novel Pd–Cu/$ZnAl_2O_4$–ZrO_2 Catalysts for Methanol Synthesis

Paweł Mierczynski · Radoslaw Ciesielski · Adam Kedziora · Marcin Zaborowski · Waldemar Maniukiewicz · Magdalena Nowosielska · Małgorzata I. Szynkowska · Tomasz P. Maniecki

Received: 8 November 2013 / Accepted: 17 January 2014 / Published online: 7 February 2014
© Springer Science+Business Media New York 2014

Abstract Monometallic Cu and bimetallic Pd–Cu catalysts promoted by ZrO_2 were prepared using impregnation method. The physicochemical properties of catalytic systems were investigated using BET, scanning electron microscopy–energy dispersive spectrometry, temperature programmed reduction-H_2, X-ray diffraction, Fourier transform infrared techniques. Catalytic activity was studied in fixed bed reactor under high pressure (4.8 MPa). The results show that addition both Pd and ZrO_2 increases the methanol yield. Zirconium oxide improved the dispersion and reducibility of the copper catalysts. The presence of adsorption species attributed to b-HCOO–Zr, b-HCO_3–Zr, m-CO_3–Zr species on the surface of ZrO_2 promoted catalysts was confirmed. The high activity of promoted palladium catalysts is explained by synergistic effect between Pd and Cu.

Keywords Methanol synthesis · Pd–Cu/$ZnAl_2O_4$–ZrO_2 · Palladium catalysts · Copper catalysts · Bimetallic catalysts · Alloy

1 Introduction

The first generation of methanol synthesis catalysts were Cr_2O_3–ZnO systems developed by BASF in 1921, but due to their low reactivity during the process involved the use of high pressures (up to 300 atm) and high temperature (about 300–400 °C). Searching new, more efficient and operating in the lower temperature and under lower pressure catalytic systems has led to the development of copper based catalysts.

One of the discoverers of a copper catalyst for methanol synthesis was Professor Blasiak, who in 1947 developed in Poland Cu/ZnO/Al_2O_3 catalyst used in the 1950s and 1960s in the high-pressure synthesis [1–3].

Research conducted by ICI in the 1960s led to the development of low-pressure methanol synthesis catalyst carried on a similar composition as the catalyst developed by Professor Blasiak [1], namely the catalyst Cu/ZnO/Al_2O_3 [4]. The low pressure methanol synthesis was carried out at the temperature range 230–260 °C under a pressure of 50–100 atm with a high conversion of CO/CO_2. Optimum efficiency of the low pressure methanol synthesis reaction had the catalyst containing 35–40 wt% CuO, 45–50 wt% ZnO and 10–20 wt% Al_2O_3 [2]. A typical industrial catalyst is a complex ternary material whose properties depend on the method of preparation, pretreatment and process conditions.

One type of catalytic materials used in methanol synthesis are Cu/ZnO/ZrO_2 and Cu/ZrO_2 catalysts showing a high activity and stability compared to Cu/ZnO systems [4–12]. The yield of the methanol synthesis catalyst supported on the ZrO_2 is comparable or even higher than the Cu/ZnO catalyst. Higher activity of copper catalysts promoted by ZrO_2 can be explained by higher specific surface area and metallic copper surface of those systems in comparison to unpromoted materials [9–12]. Besides addition of ZrO_2 results in increased adsorption of CO_2 and CO on acidic centers of ZrO_2 in relation to Cu or ZnO [4, 6]. In addition, several studies in the literature data [6, 8] confirmed that the addition of ZrO_2 increases the stability of copper catalysts.

P. Mierczynski (✉) · R. Ciesielski · A. Kedziora · M. Zaborowski · W. Maniukiewicz · M. Nowosielska · M. I. Szynkowska · T. P. Maniecki
Institute of General and Ecological Chemistry, Lodz University of Technology, Zeromskiego 116, 90-924 Lodz, Poland
e-mail: mierczyn25@wp.pl

The next group of catalytic systems for methanol synthesis are the noble metals containing catalysts. This group includes palladium catalysts supported on various supports, including e.g. alumina, silica, magnesium oxide, activated carbon, lanthanum oxide catalysts [2].

Taking into account the above informations the main goal of this work was to explain the effect of ZrO_2 and palladium on activity results and physicochemical properties of copper catalysts in methanol synthesis reaction. In order to achieve the goal of this work monometallic Cu and bimetallic Pd–Cu catalysts were prepared by wet impregnation method. The physicochemical properties of the catalytic systems were studied by BET, X-ray diffraction (XRD), temperature programmed reduction (TPR)-H_2 and Fourier transform infrared spectroscopy (FTIR) techniques. Activity tests in methanol synthesis reaction were carried out using high pressure fixed bed reactor at 260 °C and under elevated pressure 4.8 MPa.

2 Experimental Section

2.1 Catalysts preparation

Copper catalysts were prepared by wet aqueous impregnation. In order to prepare $ZnAl_2O_4$ support the following molar ratio of Zn:Al = 0.5 zinc and aluminium nitrates compounds were used. Aqueous solutions of 1 M/L zinc nitrate and 1 M/L aluminium nitrate were mixed in appreciate quantity under vigorous stirring at 80 °C. A concentrated ammonia solution was then added by dropwise addition until the pH reached values of between 10 and 11 and then the mixtures were stirred for another 30 min. The resulting fine precipitates were washed two times in deionised water and then dried at 120 °C for 15 h and calcined for 4 h at 600 °C in air. Calcination at 600 °C was chosen because such high temperature is required for creation of spinel structure and for removal of the nitrate precursor from the catalytic systems.

Supports $ZnAl_2O_4$–ZrO_2(5 %) and $ZnAl_2O_4$–ZrO_2(1 %) were prepared by impregnation method. Appreciate quantity of zirconyl nitrate(V) was taken to obtain relevant content of ZrO_2 and introduced on the carrier ($ZnAl_2O_4$) surface. The obtained material was further dried at 120 °C for 2 h and then calcined in air at 400 °C for 4 h.

Metal phase Cu and Pd was introduced on the previously prepared support surface ($ZnAl_2O_4$, 1 % ZrO_2/$ZnAl_2O_4$ and 5 % ZrO_2/$ZnAl_2O_4$) by wet impregnation using aqueous solutions of copper and palladium nitrates. The supported catalysts were then dried in air at 120 °C for 2 h and finally calcined for 4 h in air at temperatures of 400 °C. Copper and palladium loading were 20 and 2 wt%, respectively.

3 Catalysts Characterization

3.1 Specific Surface Area and Porosity (BET)

The specific surface areas of supports and catalysts were determined by the BET based on low temperature (77 K) nitrogen adsorption in a Micrometrics ASAP 2020 apparatus.

3.1.1 Temperature Programmed Reduction (TPR-H_2)

The TPR-H_2 measurements were carried out in an automatic TPR system AMI-1 in the temperature range of 25–900 °C with a linear heating rate of 10 °C/min. Samples (weight about 0.1 g) were reduced in hydrogen stream (5 % H_2–95 % Ar) with a volumetric flow rate of 40 cm^3/min. Hydrogen consumption was monitored by a thermal conductivity detector.

3.2 XRD measurements

Room temperature powder XRD patterns were collected using a PANalytical X'Pert Pro MPD diffractometer in Bragg–Brentano reflecting geometry. Copper Cu Kα radiation from a sealed tube was used. Data was collected in the range 5–90° 2θ with a step of 0.0167° and exposure per step of 27 s. Due to the fact that raw diffraction data contain some noise, the background during the analysis was subtracted using Sonneveld, E.J. and Visser algorithm. The data was then smoothed using cubic polynomial. All calculations were done using X'Pert HighScore Plus computer software.

Average crystallite size was calculated from XRD peak broadening using the Scherrer equation.

$$t = K\,\lambda/(B\cos\theta),$$

where t is the averaged dimension of crystallites, K is the arbitrary chosen Scherrer constant (0.9 in this case), λ is the wavelength of X-ray, B is the integral breadth of a reflection (in radians 2θ) located at 2θ Bragg angle.

3.3 SEM Measurements

The SEM measurements were performed using a S-4700 scanning electron microscope HITACHI (Japan), equipped with an energy dispersive spectrometer EDS (Thermo Noran, USA). Images were recorded at several magnifications using secondary electron or BSE detector. The EDS method made it possible to determine the qualitative analysis of elements present in the studied micro-area of sample surface layer on the basis of the obtained characteristic X-ray spectra. A map of the distribution of elements on the studied micro-area was made. The accelerating volt

age was 25 kV. For performing, measurements samples were coated with carbon target using Cressington 208 HR system.

3.4 Catalytic Activity Tests

Activity tests in methanol synthesis reaction were carried out using the high pressure fixed bed reactor using a gas mixture of H_2 and CO with molar ratio 2:1, respectively. Process was carried out under elevated pressure (4.8 MPa) at 260 °C and products were analyzed by GC (gas chromatograph). Before activity tests all catalysts were pre-reduced for 2 h in a flow of 5 % H_2–95 % Ar mixture at 300 °C under atmospheric pressure. The steady-state activity measurements were taken after at least 12 h on the stream. The analysis of the reaction products were carried out by an on-line GC equipped with FID detector and 10 % Carbowax 1500 on Graphpac column. The CO and CO_2 concentrations were monitored by GC chromatograph equipped with TCD detector (120 °C, 130 mA), and Carbosphere 60/80 (65 °C) column. CO conversion was calculated by the following equation:

$$CO_{conv.} = \left[\frac{(CO \text{ in feed} - CO \text{ in effluent})}{CO \text{ in feed}} \times 100\right].$$

The selectivity of the products were calculated as follows:

$$P_i \text{ selectivity} = \left(\frac{P_i \text{yield}}{\sum P_i \text{yield}}\right) \times 100,$$

P_i is the mol number of every organic product.

3.5 Diffuse Reflectance Fourier Transform Infrared Spectroscopy (DRFTIS)

IR spectra were recorded with a Thermo Scientific Nicolet 6700 FTIR spectrometer equipped with a liquid nitrogen cooled mercury cadmium telluride (MCT, HgCdTe) detector. Before analysis copper, palladium and palladium–copper catalysts supported on $ZnAl_2O_4$ were $ZnAl_2O_4$–ZrO_2(5 %) were reduced at 300 °C in gas reduction mixture 5 % H_2–95 % Ar for 1 h. After reduction, the catalysts were cooled down to 120 or 260 °C and then the reduction mixture was shifted to a mixture of approximately 1 vol.% CH_3OH in argon stream. A resolution of 4.0 cm^{-1} was used throughout the investigations. Sixty four scans were taken to achieve a satisfactory signal to noise ratio. The background spectrum was collected at 120 or 260 °C after reduction. The adsorption process involved exposure of the reduced catalysts to 1 vol.% CH_3OH in argon stream flowing at 40 cm^3/min for 30 min under atmospheric pressure. After the adsorption process, the cell was evacuated for 30 min at the same temperature in argon.

4 Results and Discussion

The specified values of catalyst surface area (BET), monolayer capacity and average pore radius are presented in Table 1 for Cu(20 %)/$ZnAl_2O_4$, Cu(20 %)/$ZnAl_2O_4$–ZrO_2(5 %) and Pd(2 %)–Cu(20 %)/$ZnAl_2O_4$–ZrO_2(5 %), respectively. 20 % Cu/$ZnAl_2O_4$ catalyst exhibited the highest specific surface area in comparison to promoted systems. The surface area of promoted catalysts decreases slightly compared to the 20 % Cu/$ZnAl_2O_4$ systems, as result of pores blocking by PdO and ZrO_2 phases. The value of monolayer capacity and average pore radius are similar for all systems and are in the range 31.3–32.5 and 1.96–2.13 nm, respectively.

The reduction behaviour of investigated systems were studied by TPR method. TPR-H_2 measurements for mono and bimetallic catalysts after calcination at 400 °C are shown on Figs. 1, 2 and 3.

Table 1 The physicochemical properties of copper supported catalysts

Catalysts	BET[a] surface area (m^2/g)	Monolayer capacity (cm^3/g)[a]	Average pore radius (nm)[a]	Cu crystallite size determined from the peak broadening (111)[b]		
				T_{red} (°C)	Cu	CuPd alloy
Cu(20 %)/$ZnAl_2O_4$	142	32.5	1.96	300	68.4	–
Cu(20 %)/$ZnAl_2O_4$–ZrO_2(5 %)	137	31.5	2.13	300	37.5	–
				900	83.8	–
Pd(2 %)–Cu(20 %)/$ZnAl_2O_4$–ZrO_2(5 %)	136	31.3	2.09	300	37.7	8.5
				900	48.2	9.6

[a] Catalysts calcined 4 h in air atmosphere at 400 °C

[b] Catalysts reduced 2 h in H_2 atmosphere at 300 or 900 °C

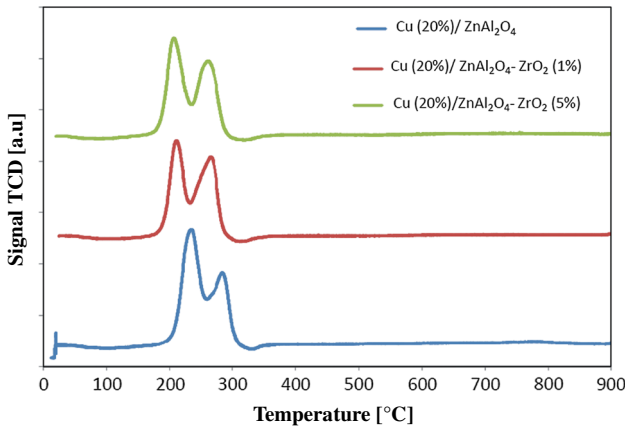

Fig. 1 TPR-H_2 patterns of Cu(20 %)/$ZnAl_2O_4$, Cu(20 %)/$ZnAl_2O_4$–ZrO_2(1 %) and Cu(20 %)/$ZnAl_2O_4$–ZrO_2(5 %) calcined at 400 °C in air for 4 h

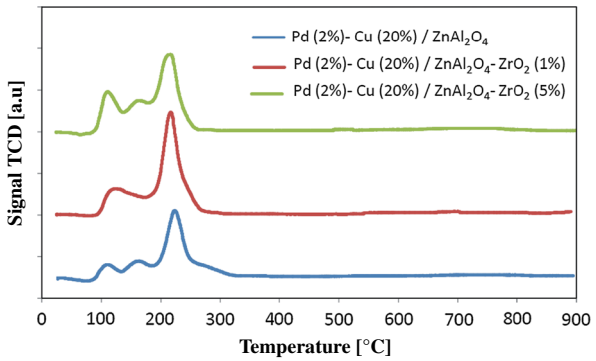

Fig. 2 TPR-H_2 patterns of Pd(2 %)–Cu(20 %)/$ZnAl_2O_4$ and Pd(2 %)–Cu(20 %)/$ZnAl_2O_4$–ZrO_2(1 %), Pd(2 %)–Cu(20 %)/$ZnAl_2O_4$–ZrO_2(5 %) calcined at 400 °C in air for 4 h

The effect of zirconium oxide addition on reduction of copper catalyst is shown on Fig. 1. The TPR-H_2 profile of Cu(20 %)/$ZnAl_2O_4$ present two partially divided effects at the temperature range 200–320 °C. Two reduction effects are connected with reduction of small and larger crystallites size of copper(II) oxide species, respectively.

Introduction of zirconium oxide on support surface caused only a slight shift of the observed hydrogen consumption peaks into lower temperature range what suggest that introduction of ZrO_2 on catalyst surface caused the decrease of metallic copper crystallite size (see Table 1). Decreasing of the metallic copper crystallize size result in growth of metallic cooper surface area and increasing the number of active centers in methanol synthesis reaction.

Similar results received Chang et al. [13]. They investigated the reduction of CuO/ZnO/ZrO_2/Al_2O_3 catalysts and also claimed that zirconium oxide improves the dispersion and reducibility of the copper catalysts. Moreover, they also confirmed that CuO/ZnO/ZrO_2/Al_2O_3 (30/50/10/10) and CuO/ZnO/ZrO_2/Al_2O_3 (30/40/20/10) have larger Cu^0 surface areas and BET surface areas than CuO/ZnO/Al_2O_3 (30/60/10) [13].

The reduction studies of copper catalysts supported on monoclinic and tetragonal ZrO_2 were performed by Aguila et al. [14]. Copper catalysts supported on monoclinic ZrO_2 exhibited two-steps reduction of copper catalysts assigned to the sequential reduction of highly dispersed Cu^{2+} species to Cu^{1+} and Cu^0. When copper was supported on tetragonal ZrO_2 the TPR peaks were broad and less defined. On the TPR profiles of those systems maxima between 150 and 250 °C attributed to highly dispersed copper oxide species were visible. The copper catalyst with high copper loading exhibited additional reduction effect visible at 296 °C which was attributed to the reduction of CuO bulk. The high temperature reduction effects is much smaller than the one observed on the 6 % Cu on monoclinic ZrO_2, which indicates a better dispersion of copper oxide phase on the tetragonal structure of ZrO_2 [14].

The reduction behaviour of copper catalysts deposited on various support such as : γ-Al_2O_3, ZrO_2 and ZrO_2/γ-Al_2O_3 was investigated also by Bellido and Assaf [15]. TPR measurements performed for copper catalysts supported on γ-Al_2O_3 showed that all catalysts reduce in one reduction step whose intensity increased with the copper load. Results of the TPR analyses of the CuO/ZrO_2 catalysts showed that catalytic systems were reduced in two reduction steps attributed to the reduction of highly dispersed CuO and/or Cu^{2+} ions in octahedral environmental (first peak) and with bulk CuO (second peak). However, in the case of copper catalysts supported on binary oxide ZrO_2/γ-Al_2O_3 one reduction peak was visible on the reduction profile for catalysts with low copper content. Increase of copper loading caused the appearance of additional reduction peak at lower reduction temperature suggesting the increase the level of interaction between the copper species and the oxygen vacancies [15].

Figure 2 present the influence of palladium on the reduction behaviour of Cu(20 %)/$ZnAl_2O_4$ catalyst. TPR curve recorded for Pd(2 %)–Cu(20 %)/$ZnAl_2O_4$ showed three reduction steps. The first effect is assigned to PdO reduction, the next two observed effects are connected as for the copper catalyst with copper oxide species reduction. The shift of the reduction effects attributed to copper oxide reduction steps is explained by the spillover effect occurring between metallic palladium and CuO. It is well known that hydrogen dissociate on palladium surface and then absorbs hydrogen which flows from palladium to the copper oxide causing its easier reduction.

The reduction of bimetallic Pd–Cu/γ-Al_2O_3 catalyst made by impregnation was studied by Sá and Vinek [16]. They observed on the TPR profile a reduction peak with two maxima at 103 °C and at 146 °C. The first hydrogen

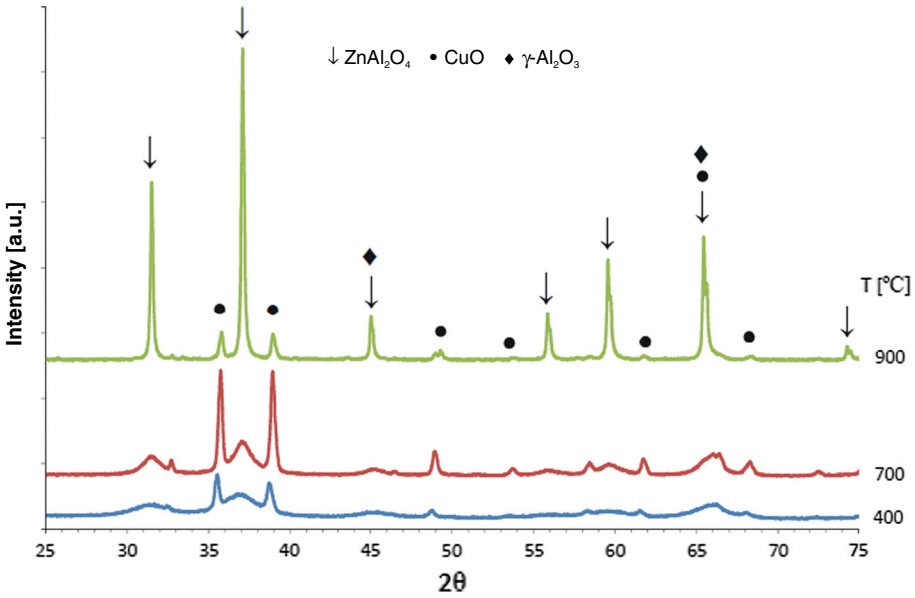

Fig. 3 XRD profiles of Cu(20 %)/$ZnAl_2O_4$ catalyst calcined in air at 400, 700 and 900 °C for 4 h

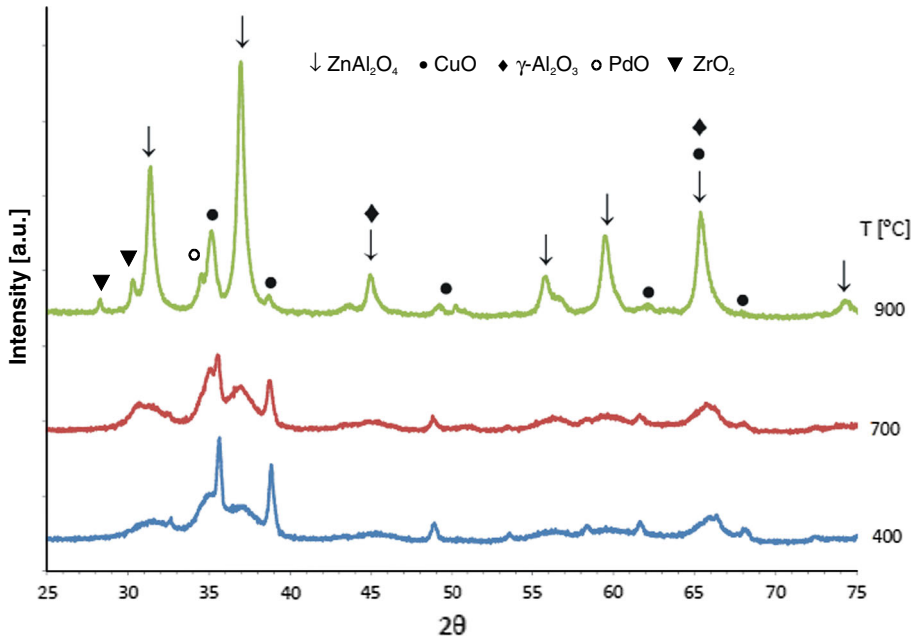

Fig. 4 XRD profiles of Pd(2 %)–Cu(20 %)/$ZnAl_2O_4$–ZrO_2(5 %) catalyst calcined in air at 400, 700 and 900 °C for 4 h

consumption peak was attributed to the reduction of palladium–copper mixed oxide species [17] resulting from migration of the metals during calcination. The second peak was assigned to the reduction of CuO to Cu_2O and Cu^0. Authors claimed that the formation of an alloy can also shift the reduction temperatures of the metals oxides [17].

Figure 2 displays also the influence also the ZrO_2 addition on the reduction behaviour of copper catalysts. To better demonstrate the investigative effects the first TPR curve showed the reduction of Pd(2 %)–Cu(20 %)/$ZnAl_2O_4$ catalyst. On the TPR profile recorded for this system we observed the same reduction stage as for presented above palladium–copper catalyst. Addition of zirconium oxide caused the increase of the reduction effect intensity attributed to the reduction of PdO. Any others differences in the reduction behaviour of palladium–copper catalysts did not occur.

The reduction studies of 7Cu/3Zn and 7Cu/3Zn/1Zr catalysts promoted by palladium were performed by Schuyten et al. [18]. In their work the presence of palladium influenced the reduction regardless of CuO particle size, dispersion of copper, and interactions with ZrO_2. They also observed the lower reduction temperature of

palladium catalysts compared to 7Cu/3Zn and 7Cu/3Zn/1Zr and this result they explained by a well-known spill-over mechanism involving hydrogen adsorption and dissociation on Pd^0 crystallites, followed by activated hydrogen migration to CuO.

The phase composition studies of calcined and reduced catalysts at various temperature were studied by XRD techniques to elucidate the interaction between active component and support. XRD measurements of calcined monometallic Cu(20 %)/$ZnAl_2O_4$ catalysts are given on Fig. 3. On the XRD diffractograms recorded for copper catalysts calcined at various temperature we can easily observed CuO, γ-Al_2O_3 and $ZnAl_2O_4$ phases. The increase of the calcination temperature cause only the growth of sample crystallinity.

In the next step we studied the phase composition of palladium–copper catalysts promoted by 5 wt% of zirconium oxide. Figure 4 displays the XRD measurements of Pd(2 %)–Cu(20 %)/$ZnAl_2O_4$–ZrO_2(5 %) catalysts calcined at 400, 700 and 900 °C. The XRD curve of Pd(2 %)–Cu(20 %)/$ZnAl_2O_4$–ZrO_2(5 %) catalyst calcined at 400 °C in air for 4 h showed the presence of following phases: PdO, CuO, γ-Al_2O_3 and $ZnAl_2O_4$ whose intensity increases with increasing of the calcination temperature.

This is caused by increasing the size of the crystallites as a result of calcination process carried out at high temperatures. Additionally, the XRD curve of this system calcined at 900 °C presents the occurrence of ZrO_2 structure which was not observed at lower calcination temperature. Decrease of the intensity of the diffraction peaks originating from CuO and increasing of reflexes coming from $ZnAl_2O_4$ spinel structure for palladium–copper doped catalysts calcined at higher temperature (see Fig. 4) in comparison to catalyst calcined at lower temperature indicating the formation of new spinel $CuAl_2O_4$ structure. It can therefore be assumed that the high calcination temperature (900 °C) caused the formation of new spinel $CuAl_2O_4$, which crystallized in the same crystallographic structure AB_2O_4 as $ZnAl_2O_4$ system, in accordance with following equation:

$$\gamma\text{-}Al_2O_3 + CuO \rightarrow CuAl_2O_4.$$

The confirmation of this suggestion was the appearance of additional reduction stage situated at high temperature range in the case of Cu/$ZnAl_2O_4$ catalysts calcined at 700 or 900 °C. This high reduction profile is connected with copper aluminate spinel structure reduction. The precise description of the reduction behaviour of copper catalysts and their phase composition are given in our previous work [19].

The XRD measurements of calcined CuO/ZnO/Al_2O_3 and CuO/ZnO/ZrO_2/Al_2O_3 catalysts were performed by Chang et al. [20, 21]. The authors also did not observe diffraction peaks stem from ZrO_2 phase for catalysts calcined at 350 °C for 4 h. Additionally, the diffraction peaks of CuO and ZnO were weakened and even disappeared as ZrO_2 was introduced into CuO/ZnO/Al_2O_3 system.

In the next stage of our investigation we would like to understand the mechanism of the reduction of palladium–copper catalyst, so we decided to carry out the XRD measurements of reduced in hydrogen at 300 and 900 °C of copper, palladium–copper and palladium–copper promoted by zirconium oxide catalysts. On the Fig. 5 we can easily observed the XRD curves of copper supported catalysts. The phase composition studies performed for this systems allow to confirm the reduction mechanism described in

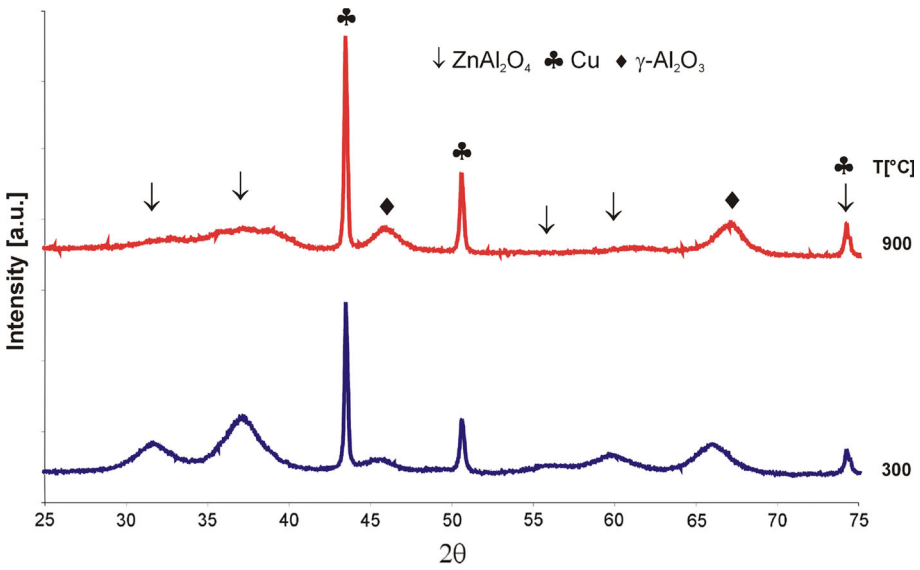

Fig. 5 XRD profiles of Cu(20 %)/$ZnAl_2O_4$ catalyst reduced in hydrogen at 300 and 900 °C for 2 h

reduction part of this work. On the diffractograms recorded for this catalysts we could easily detected metallic Cu, $ZnAl_2O_4$ and γ-Al_2O_3. It is worth emphasizing that reduction at high temperature caused only the growth of catalyst crystallinity.

Very interesting result we obtained for Pd(2 %)–Cu(20 %)/$ZnAl_2O_4$–ZrO_2(5 %) (see Fig. 6). On the XRD diffraction curve of Pd(2 %)–Cu(20 %)/$ZnAl_2O_4$–ZrO_2(5 %) catalyst reduced at 300 °C we observed apart from Cu, $ZnAl_2O_4$ and γ-Al_2O_3 phases additional PdCu phases.

The presence of PdCu alloy phase confirmed the interaction of Pd and CuO during reduction process and can explained the shift of TPR result observed on the reduction curves recorded for palladium catalysts. The increasing of reduction temperature to 900 °C result in growth of reflection intensities attributed to Cu and PdCu phases and the appearance of ZrO_2 structure.

According to Murach [22] the ZnO reduction in hydrogen atmosphere starts above 1,100 °C, whereas the reduction of the same compound in coke take place at lower temperature at about 900 °C. The confirmation of this claim were the XRD results obtained for monometallic copper catalysts after reduction at 300 and 900 °C. On the diffraction curves recorded at those temperature we did not observe any alloying process which could be attributed to brass phase formation.

Kugai et al. [23] studied bimetallic palladium–copper supported catalyst in WGS reaction. The authors also confirmed by EXAFS technique that alloy between copper and palladium is formed after reduction and Pd helps to keep metallic copper in reduced state during the reaction [24].

Schuyten et al. [18] investigated Pd–CuO/ZnO/ZrO_2 catalysts for hydrogen production by methanol partial oxidation and they investigated the physicochemical properties using XPS, XRD, EXAFS, BET and TPR-H_2 methods. The oxidation state of copper in the prepared catalysts were studied using the Cu K edge XAS for calcined in air at 500 °C for 2 h, reduced at 300 °C and for catalysts being after the reaction. Authors also found that Pd–Cu can form alloy at reduction temperatures of 300 °C or below. It is worth to emphasize that mixture if copper was maintained as Cu^0 and/or Cu^+, palladium remained in a reduced alloy state regardless of temperature and reaction.

In the next step of our investigation we decided to calculate the composition of PdCu alloy. We used Vegard's law to determine the composition of our alloy [25]. Vegard's law is an approximate empirical rule which holds that a linear relation exists, at constant temperature, between the crystal lattice constant of an alloy and the concentrations of the constituent elements. The CuPd alloy is solid solution with cubic structure. In this case a linear combination of lattice spacing of the individual metal components and their mole fraction is given by equation:

$$a_{CuPd} = x_{Pd}a_{Pd} + (1 - x_{Pd})a_{Cu},$$

where a is the lattice constant, and x is the mole fraction. Through the use of the lattice constant of pure Cu and that of the alloying atom (Pd), the lattice constant of the remainder of the alloy compositions between 0 and 100 can be estimated using Vegard's law. By the use of the simulated lattice spacing of Pd and Cu, Vegard's law was used to predict the mole fraction of Pd with lattice constant of

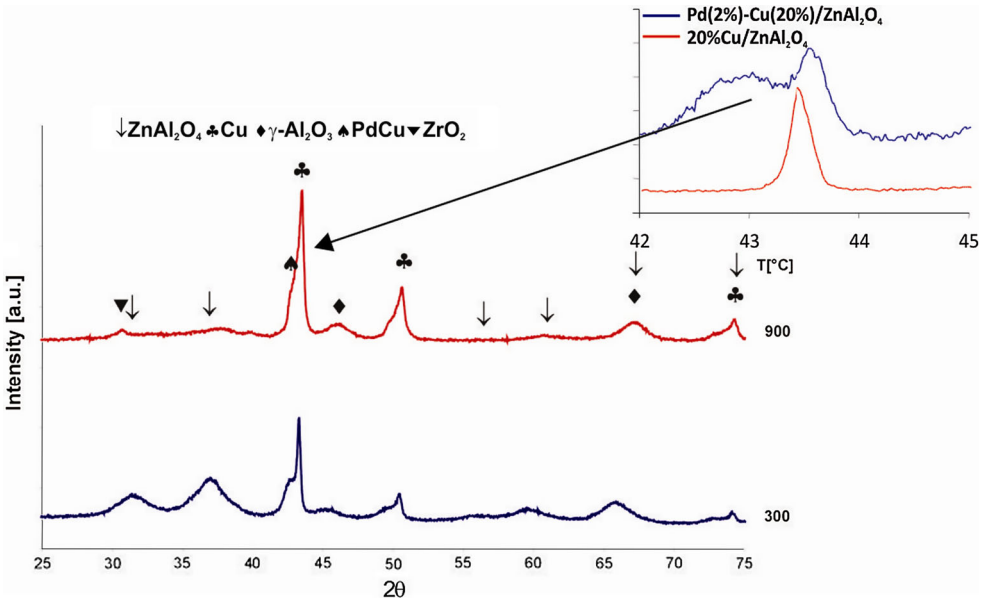

Fig. 6 XRD profiles of Pd(2 %)–Cu(20 %)/$ZnAl_2O_4$–ZrO_2(5 %) catalyst reduced in hydrogen at 300 and 900 °C for 2 h

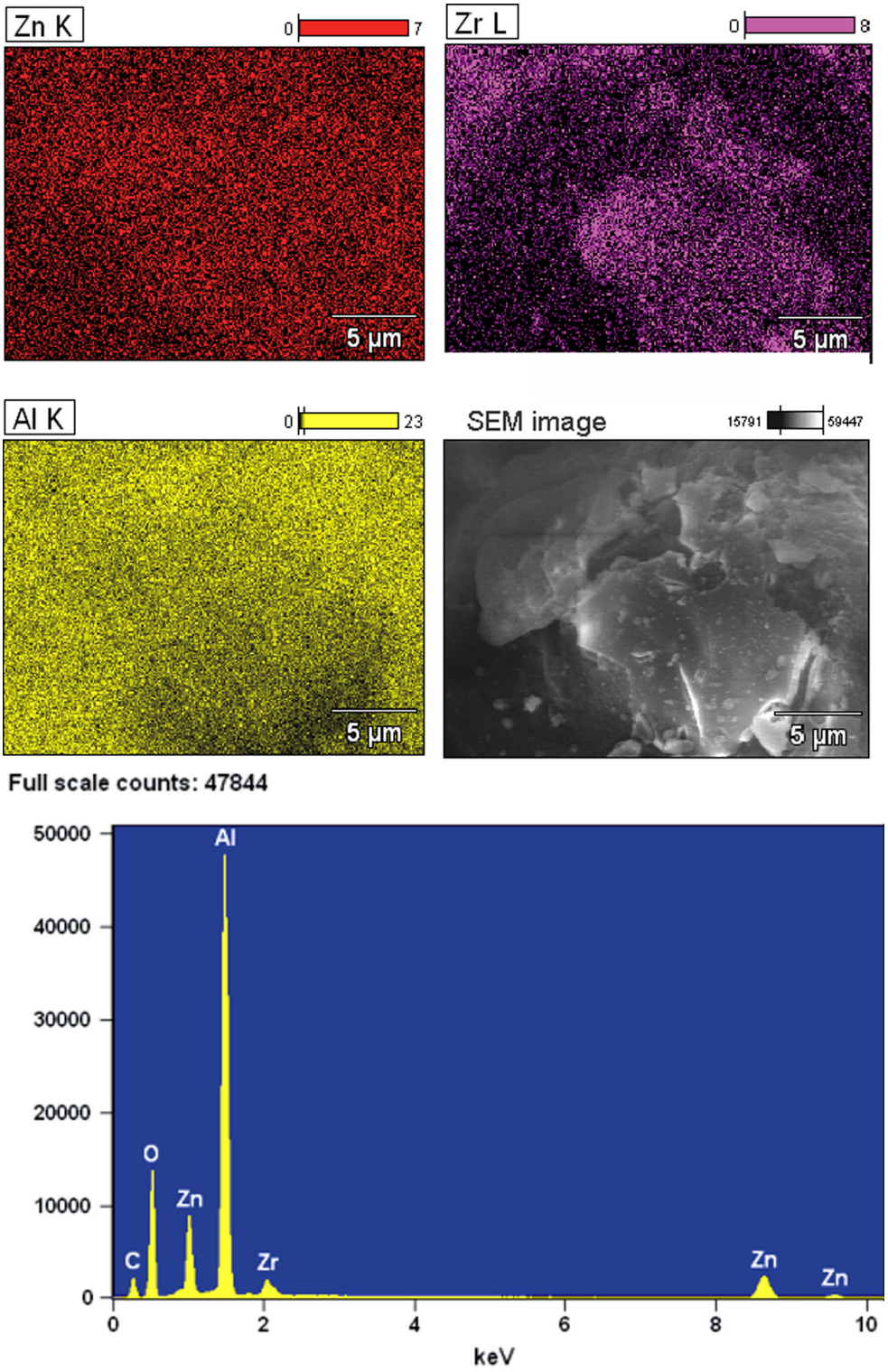

Fig. 7 The results of SEM–EDS measurements for $ZnAl_2O_4$–ZrO_2(5 %) after calcination at 400 °C

PdCu alloy. The percentage of palladium in the alloy was 17.8 %.

Sá and Vinek [16] investigated the phase composition studies of Pd–Cu/γ-Al_2O_3 (the metal content was as follows: Pd = 5 wt%, Cu = 1.25 wt%) catalyst prepared using impregnation method after calcination in air at 450 °C and reduction at the same temperature. The XRD measurements showed that only after reduction the diffraction peaks attributed to Pd on the diffraction curve are visible. Authors observed the shift the Pd (1 1 1) and (2 0 0) reflexes to higher 2θ values indicating an insertion of copper in palladium.

In the literature data [16, 26, 27] can be found that Pd–Cu alloy with various composition PdCu and $PdCu_3$ can be created, with Cu normally segregating onto the surface of the nanoparticles. This selective behaviour of Cu is explained by lower surface free energy and by the exothermicity of the Pd–Cu alloy formation process and the difference in the atomic radii of Cu and Pd [28].

Sun et al. [28] claims that the reduction at 500 °C or below is not sufficient to complete the formation of the alloy of Pd–Cu. They concluded that low reduction temperature caused generation separated particles of Pd and later the reduced Cu species diffuse into the Pd particles at higher temperatures, resulting in the formation of bimetallic Pd–Cu particles.

Schuyten et al. [18]. studied also the phase composition of calcined 7Cu/3Zn and 7Cu/3Zn/1Zr catalysts promoted by palladium. On the diffraction patterns of palladium catalysts only broad lines corresponding to CuO and ZnO were clearly identifiable. However authors did not observe any peaks which could be assigned to palladium or zirconium compounds.

The most apparent feature is the significant broadening of CuO and ZnO lines in patterns of the promoted ZrO_2 catalysts. The lack of ZrO_2 XRD peaks in patterns in promoted CuO/ZnO catalysts has been attributed to a highly disordered or amorphous state, or small crystallite size, and low wt% of the ZrO_2 phase [18, 29].

A scanning electron microscope (SEM) S-4700 (HITACHI, Japan), equipped with an EDS (Thermo Noran, USA) was employed to characterize the morphology and determination of elemental distribution of support [$ZnAl_2O_4$–ZrO_2(5 %)]. The results of SEM–EDS measurements for $ZnAl_2O_4$–ZrO_2(5 %) supported catalyst after calcination 4 h in air atmosphere at 400 °C are shown in Fig. 7. The magnification was equal 5,000. The distribution of aluminum, zinc and zirconium are also shown in Fig. 7. The EDS images collected from the surface showed that the distribution of ZrO_2 on the $ZnAl_2O_4$ support surface is inhomogeneous. On the SEM image presented in the same picture the various particles size of the $ZnAl_2O_4$–ZrO_2(5 %) system could be found. The SEM results confirmed that the particle size are in the range 0.1–20 μm.

The CO hydrogenation to methanol was also studied in this work. The results of activity tests of monometallic copper, copper promoted by ZrO_2 and bimetallic palladium–copper promoted by ZrO_2 catalysts in methanol synthesis reaction carried out at 260 °C expressed in g CH_3OH/kg_{cat}·h are given in Table 2. It is worth emphasizing that only two organic products were formed during studied reaction: methanol and methane. The formation of other oxygenates were not observed. Carbon monoxide conversion and selectivity to carbon dioxide, methanol and methane obtained in the studied reaction are shown in the same Table 2. The activity results gave evidence that the highest methanol formation and carbon monoxide conversion had Pd(2 %)–Cu (20 %)/$ZnAl_2O_4$–ZrO_2(5 %) system. A little bit lower activity exhibited copper catalyst promoted by zirconium oxide. It is worth noticing that introduction of both Pd and ZrO_2 increases the methanol yield and conversion of CO in comparison to monometallic Cu(20 %)/$ZnAl_2O_4$ catalyst. Activity results can suggest that increasing the dispersion of copper after introduction of ZrO_2 and the presence of spillover effect between Pd and Cu as evidenced by the formation of alloy compound PdCu resulting in an increased activity of a copper catalyst Cu(20 %)/$ZnAl_2O_4$.

Additionally, the occurrence of PdCu alloy lead to an increase in selectivity of the catalyst in methanol synthesis reaction. Base on the results of this work we could assumed that the role of Pd in the promotion effect was attributed to the promotion of hydrogen activation due to the hydrogen spillover effect.

In order to clarify and understanding of the differences in catalytic activity of copper supported catalysts in methanol synthesis reaction the surface adsorbed species formed during methanol adsorption on catalysts surface were investigated by IR technique. Figures 8 and 9 displays the IR spectra taken after the exposure of copper supported catalysts to a 1 vol.% CH_3OH in argon stream under atmospheric pressure at 120 and 260 °C, respectively. The IR spectra collected for Cu(20 %)/$ZnAl_2O_4$ catalyst (Fig. 8a) showed that copper formate (HCOO–Cu: 2925, 2850, 1620, 1364, and 1350 cm^{-1}), zinc formate (HCOO–Zn: 2970, 2880, 2700, 1591, 1372, and 1365 cm^{-1}), carbonate (CO_3^{2-} : 1620, 1570–1440, and 1220 cm^{-1}), zinc methoxide (CH_3O–Zn: 2936, 2919, 2825, 1470, 1200 and 1060 cm^{-1}), copper methoxide (CH_3O–Cu: 1443 and 1350 cm^{-1}) and

Table 2 The reaction results for methanol synthesis from CO/H_2 over promoted and unpromoted 20 % Cu/$ZnAl_2O_4$ catalysts

Catalysts	CO conversion (%)	Yield (g CH_3OH/kg_{cat}·h)	Selectivity to organic products (C mol%)		
			CO_2 (%)	CH_4 (%)	MeOH (%)
Cu (20 %)/$ZnAl_2O_4$	10.9	49	41	3	56
Cu(20 %)/$ZnAl_2O_4$–ZrO_2(5 %)	14	172	7	3	90
Pd(2 %)–Cu(20 %)/$ZnAl_2O_4$–ZrO_2(5 %)	19.5	194	7	1.5	91.5

Reaction condition: weight of catalyst = 2 g, H_2/CO ratio in the feed = 2, temperature = 260 °C, total pressure = 4.8 MPa

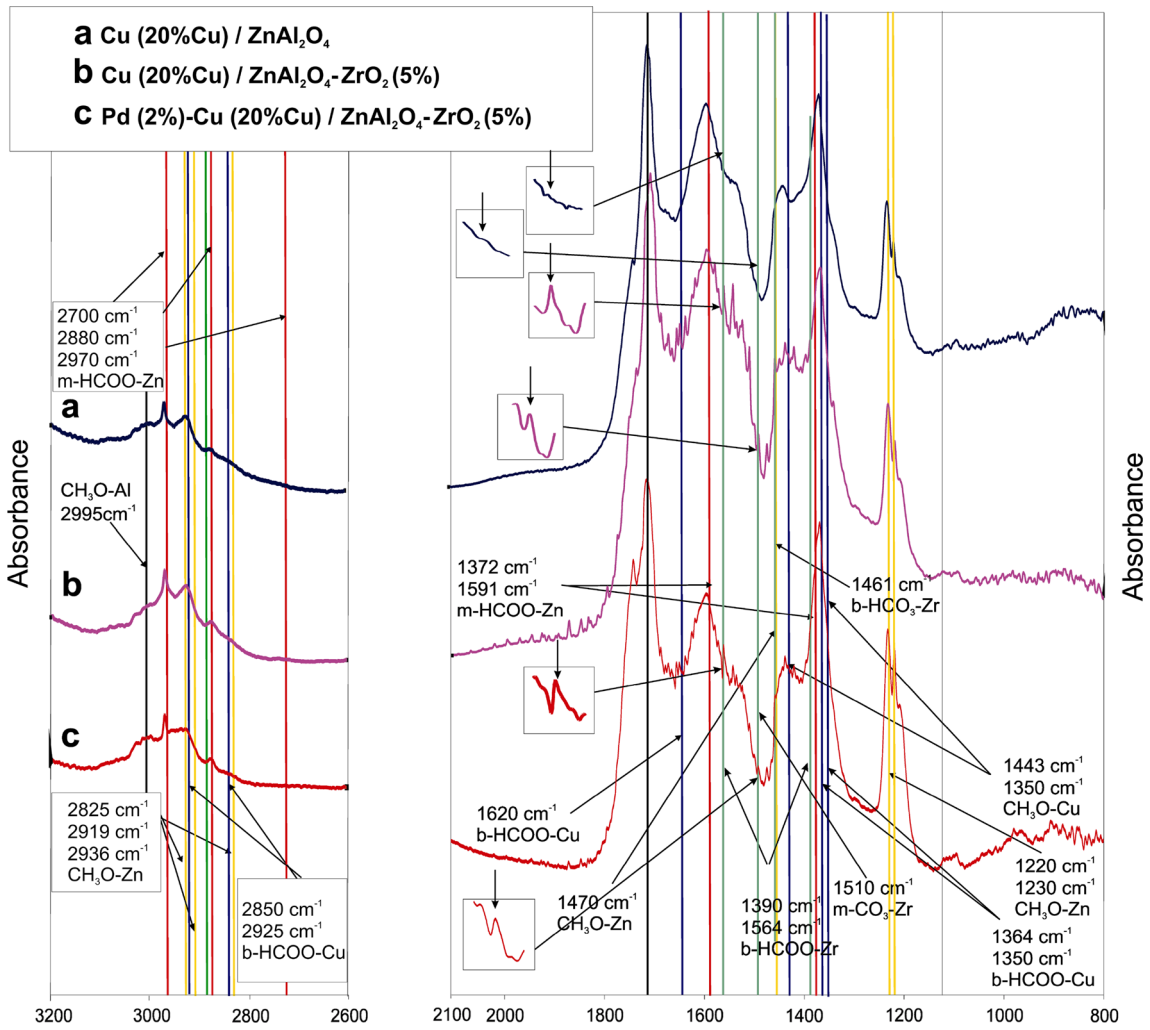

Fig. 8 Infrared spectra of adsorbed species taken after reduction at 300 °C in the 5 % H_2–95 % Ar mixture and exposure of the following catalytic systems: (*a*) Cu(20 %)/$ZnAl_2O_4$, (*b*) Cu(20 %)/$ZnAl_2O_4$–ZrO_2(5 %), and (*c*) Pd(2 %)–Cu(20 %)/$ZnAl_2O_4$–ZrO_2(5 %) to a 1 vol.% methanol–argon mixture at 120 °C

aluminium methoxide (CH_3O–Al: 2995, 1020–1100 cm^{-1}) species were adsorbed on its surface. Additionally, on the IR spectrum the appropriate bands attributed to gaseous CO (2183 cm^{-1}), gaseous CO_2 (2359 and 2320 cm^{-1}) and hydroxyl species were also detected after methanol adsorption. Those results were not presented in this work because we wanted to visualization other forms of surface-adsorbed species.

The similar measurements were carried out in our previous work [19, 30] and we observed the same surface species for Cu(20 %)/$ZnAl_2O_4$–ZrO_2(5 %) and Pd(2 %)–Cu(20 %)/$ZnAl_2O_4$–ZrO_2(5 %) (see Figs. 8, 9b, c, respectively). One of the differences observed for the ZrO_2 containing systems was the appearance of additional bands positioned at 1390, 1461, 1510, 1564 cm^{-1} attributed to b-HCOO–Zr, b-HCO_3–Zr, m-CO_3–Zr, b-HCOO–Zr species, respectively [31]. The occurrence of these surface species on the catalyst surface after methanol exposure confirms the promotion effect of ZrO_2 on CO hydrogenation towards methanol formation. This result can also explain the differences observed in catalytic activity for the studied copper supported systems. It is well known that formate species formed on the copper or support surface plays pivotal role in methanol synthesis reaction. The formate species formed on the support surface or on the perimeter between palladium and support would play important role in the methanol synthesis as those formed on supported copper catalysts.

It is worth mentioning that increasing of the adsorption temperature from 120 to 260 °C did not cause significant changes in IR spectra, the same surface species on the catalysts surface were detected. On the IR spectrum collected at 260 °C we observed the decrease of the band positioned at 1720 cm^{-1} attributed to the CH_3OH and simultaneous increasing the intensity assigned to the bidentate and monodentate formate species which are the intermediate species in methanol synthesis reaction.

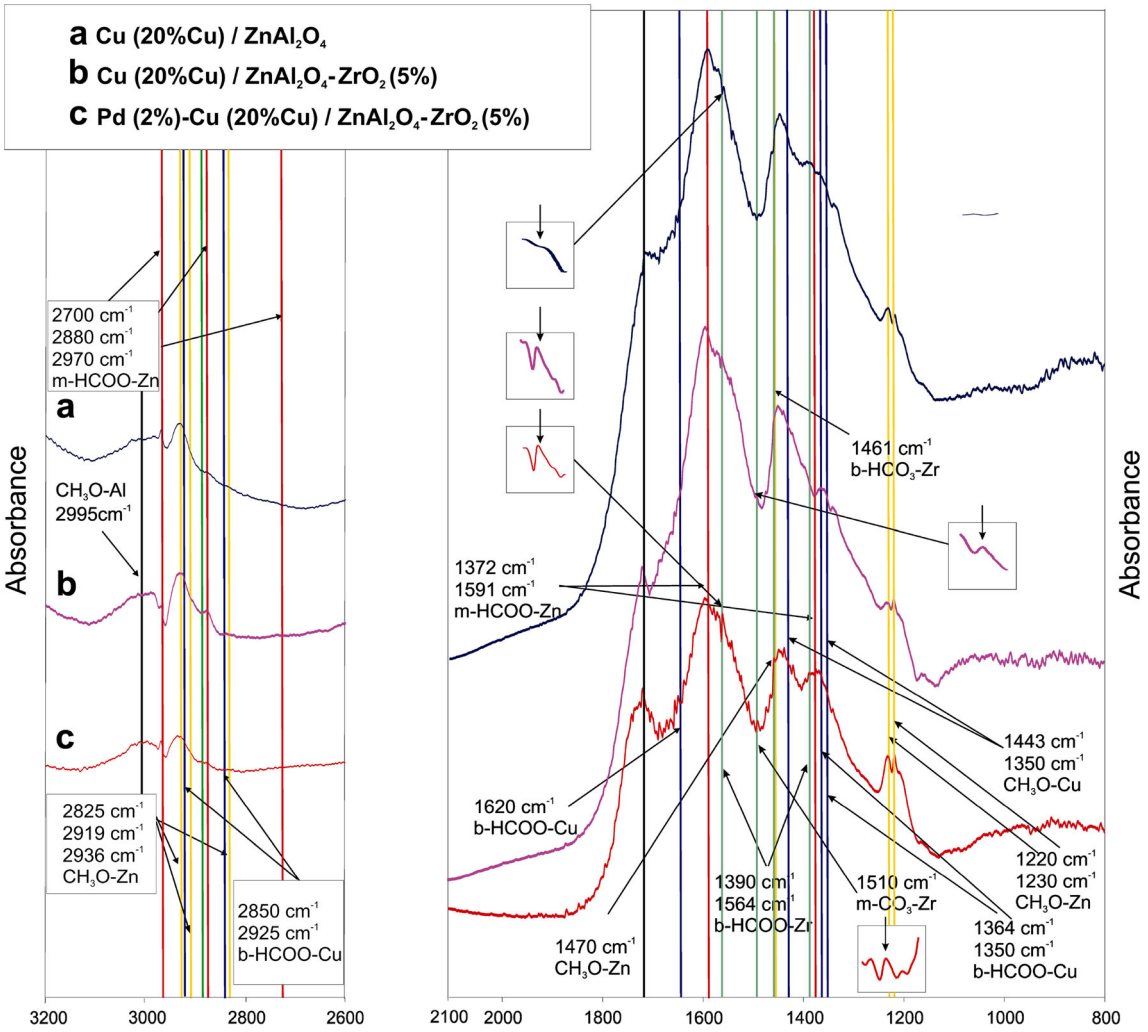

Fig. 9 Infrared spectra of adsorbed species taken after reduction at 300 °C in the 5 % H_2–95 % Ar mixture and exposure of the following catalytic systems: (*a*) Cu(20 %)/$ZnAl_2O_4$, (*b*) Cu(20 %)/$ZnAl_2O_4$–ZrO_2(5 %), and (*c*) Pd(2 %)–Cu(20 %)/$ZnAl_2O_4$–ZrO_2(5 %) to a 1 vol.% methanol–argon mixture at 260 °C

It is well known in the literature data that Zr–formate species take part in the methanol synthesis reaction and the concentration of those species are essential for achieving high catalytic activity.

According to Jung and Bell [32] the promotion of copper catalysts by ZrO_2 may lead to an increase in the quantity of intermediate products formed during methanol synthesis. What directly improve the activity of promoted copper catalysts in methanol synthesis reaction.

Wang et al. [33] claimed that zirconia is an excellent promoter or support for the methanol synthesis catalyst. The authors reported that promotion of copper catalysts by zirconia leads to improvement of catalytic activity and selectivity towards methanol, explaining this fact to enhance the dispersion of copper after the introduction of zirconium oxide.

The intermediate formate like species are formed on the surface of ZrO_2 primarily via the following process $CO_{(g)} + HO–Zr \rightarrow HCOO–Zr$. It can be also noted that formate like species could be formed also on the copper surface and spill over onto the surface of ZrO_2 [34].

Base on the IR and activity investigations carried out on catalytic systems we propose the comprehensive scheme of possible reaction routes which can take place during the hydrogenation of carbon monoxide. The possible reactions which can take place during methanol synthesis are given on Fig. 10. At the first stage of the reaction gaseous CO adsorb on the catalysts surface and react with two kinds of the surface species. The first possible reaction is methanation of CO. The second possible reaction route is oxidation of CO surface species by atomic oxygen surface species what cause the carbon dioxide formation. Created carbon dioxide can in the next step of reaction undergo hydrogenation or oxidation to form a surface carboxyl or carbonate groups, respectively. Carboxyl group undergo transformation to carbon monoxide and hydroxyl surface species or bidentate formate species.

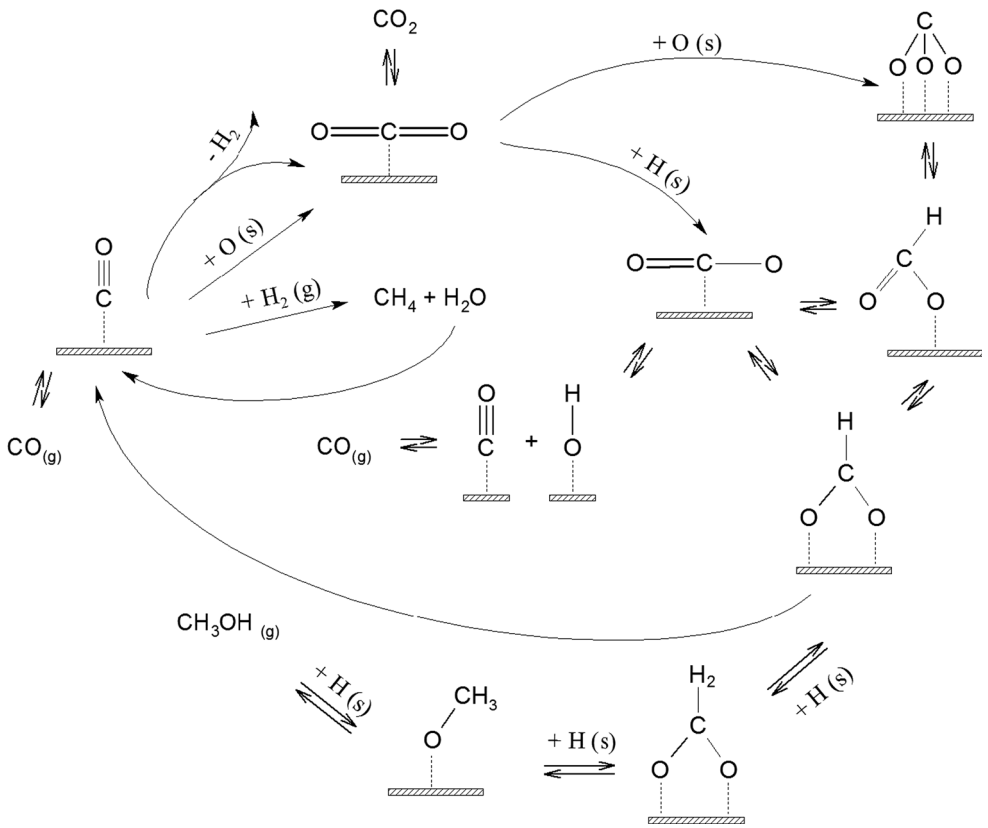

Fig. 10 Possible reaction routes which can take place during the hydrogenation of carbon monoxide

Whereas the carbonate surface species can be hydrogenated to monodentate formate species, which can then may be transform to bidentate formate surface species. It should be noted that monodentate formate can also transform to carboxyl group [4, 31].

The created from carboxyl or carbonate group bidentate formate surface species can undergo further reaction with surface hydrogen and create methoxy species and then methanol. The other way of the reaction with bidentate formate participating is decomposition reaction of previously formed b-$HCOO^-$ to carbon monoxide and hydroxyl species.

The presented scheme suggest that bidentate formates are directly hydrogenated to methanol through methoxy species and b-$HCOO^-$ groups are the intermediate species in methanol synthesis reaction. Additionally, formation of those species determines the rate of methanol synthesis [19].

5 Conclusion

Copper and palladium–copper catalysts supported on $ZnAl_2O_4$ or $ZnAl_2O_4$–ZrO_2 were prepared using impregnation method and tested in CO hydrogenation. The reduction studies confirmed that both ZrO_2 and Pd addition facilitate the reduction of CuO species. ZrO_2 addition improves the metallic Cu dispersion on the catalyst surface. Whereas, promotion of copper catalyst by palladium facilitate the copper species reduction by spillover effect between Pd and CuO. The alloy PdCu formation during reduction process in the case of palladium promoted catalyst was confirmed by XRD method. The presence of additional surface species b-HCOO–Zr, b-HCO_3–Zr, m-CO_3–Zr adsorbed on the promoted ZrO_2 catalysts surface after methanol exposure were confirmed using FTIR method. All mentioned suggestion allow to explain the activity of studied systems in methanol synthesis which can be described by following order: Pd(2 %)–Cu(20 %)/$ZnAl_2O_4$–ZrO_2(5 %) > Cu(20 %)/$ZnAl_2O_4$–ZrO_2(5 %) > Cu(20 %)/$ZnAl_2O_4$.

Acknowledgments Partially financed from Grant number 0680/B/H03/2011/40 is gratefully acknowledged.

References

1. Blasiak E (1947) Polish Patent PRL 34000
2. Bartholomew CH, Farrauto JF (2006) Fundamentals of industrial catalytic processes. Wiley Interscience, New York
3. Skrzypek J, Słomczyński J, Ledakowicz ST (1994) Methanol synthesis—science and engineering. Polish Scientific Publishers, Warsaw
4. Rhodes MD, Bell AT (2005) J Catal 233:198

5. Coteron A, Hayhurst AN (1994) Chem Eng Sci 49:209
6. Bell A (2001) Stud Surf Sci 136:13
7. Grzybowska B, Słoczynski J, Grabowski R, Samson K, Gressel U, Wcisło K, Gengembre L, Barbaux Y (2002) Appl Catal A 230:1
8. Lachowska M, Skrzypek J (2004) React Kinet Catal Lett 83:269
9. Köppel RA, Baiker A, Schild C, Wokaun A (1991) Stud Surf Sci Catal 63:59
10. Nitta Y, Suwata O, Ikeda Y, Okamoto Y, Imanaka T (1994) Catal Lett 26:345
11. Chen H, Yin A, Guo X, W-l Dai, Fan K-N (2009) Catal Lett 131:632
12. Fujitani T, Saito M, Kanai Y, Kakumoto T, Watanabe T, Nakamura J, Uchijima T (1994) Catal Lett 25:271
13. Chang C-C, Chang C-T, Chiang S-J, Liaw B-J, Chen Y-Z (2010) Int J Hydrog Energy 357:675
14. Aguila G, Guerrero S, Araya P (2009) Catal Commun 9:2550
15. Bellido JDA, Assaf EM (2009) Fuel 88:1673
16. Sá J, Vinek H (2005) Appl Catal B 57:247
17. Batista J, Pintar A, Mandrino D, Jenko M, Martin V (2001) Appl Catal A 206:113
18. Schuyten S, Guerrero S, Miller JT, Shibata T, Wolf EE (2009) Appl Catal A 352:133
19. Mierczynski P, Maniecki TP, Chalupka K, Maniukiewicz W, Jozwiak WK (2011) Catal Today 176:21
20. Chang CC, Wang JW, Chang CT, Liaw BJ, Chen YZ (2012) Chem Eng J 192:350
21. Chang CC, Chang CT, Chiang SJ, Liaw BJ, Chen YZ (2010) Int J Hydrog Energy 35:7675
22. Murach NN (1947) Sprawochnik metallurga po tsvetnym metallam tom II Metallurgia tiazchelyh metallov. Metalurgizdat, Moscow, p 514
23. Kugai J, Miller JT, Guo N, Song C (2011) J Catal 277:46
24. Fox EB, Velu S, Engelhard MH, Chin YH, Miller JT, Kropf J, Song CS (2008) J Catal 260:358
25. Sonwane CG, Wilcox J, Ma YH (2006) J Phys Chem B 110:24549
26. Fernandez-Garcia M, Anderson JA, Haller GL (1996) J Phys Chem 100:16247
27. Benedetti A, Fagherazzi G, Pinna F, Rampazzo G, Selva M, Strukul G (1991) Catal Lett 10:215
28. Sun K, Liu J, Nag NK, Browing ND (2002) J Phys Chem B 106:12239
29. Agrell J, Birgersson H, Boutonnet M, Melian-Cabrera I, Navarro RM, Fierro JLG (2003) J Catal 219:389
30. Mierczynski P, Vasilev K, Mierczynska A, Maniukiewicz W, Maniecki TP (2013) Top Catal 56:1015
31. Fisher IA, Bell AT (1998) J Catal 178:153
32. Jung KT, Bell AT (2002) Catal Lett 80:63
33. Wang W, Wang S, Ma X, Gong J (2011) Chem Soc Rev 40:3703
34. Jung K-D, Bell AT (2000) J Catal 193:207